J|A|C|S ARTICLES

Published on Web 07/09/2009

Fabrication and Electronic Characterization of Single Molecular Junction Devices: A Comprehensive Approach

Jianfeng Zhou, Fan Chen, and Bingqian Xu*

Molecular Nanoelectronics, Faculty of Engineering & Nanoscale Science and Engineering Center, University of Georgia, Athens, Georgia 30602

Received February 13, 2009; E-mail: bxu@engr.uga.edu

Abstract: We demonstrated a new comprehensive method to combine scanning probe microscopy (SPM) nanolithography and modified SPM break junction techniques to fabricate and characterize single molecular break junction devices. By patterning alkanedithiol and alkanediamine molecules in the alkanethiol template and measuring the conductance of the two kinds of molecular junctions, we have shown the following: (1) the new "stretch-hold" approach produced four groups of conductance values for each molecular junction, for the first time realizing the less populated conductance values that correspond to different contact configurations; (2) the electronic transport mechanism for such molecular junctions is electronic tunneling with similar decay constants for each conductance group of the same kind of molecules. The conductance differences among different groups are due to the molecule−electrode contact configuration difference, which was shown by the extrapolated contact resistances. This new approach also allows one to eliminate, or at least minimize, the variations of experimental conditions and enables the measurement of multiple molecules under the same experiment with exactly the same experimental conditions.

Introduction

One of the ultimate goals of molecular electronics is the construction of electronic circuit devices from individual molecules,[1,2] and electronic transport through single molecules is crucial to such molecular devices as molecular wires, rectifiers, and transistors. Great advances have been made in measuring the electrical conductance of different molecules with various techniques,[3−9] among which the scanning probe microscopy based break junction technique (SPMBJ) was widely used to study single molecule conductance by covalently binding the molecule wires to the metal tip and substrate electrodes.[10] With this technique, thousands of molecular junctions are repeatedly formed in a short time. The conductance histograms can be constructed from the individual measurements for the statistic analysis of the electron transport properties of different molecules. The well-defined peaks shown in the constructed histograms represent the most probable microscopic configurations of the molecular junctions, and the peaks are located at integer multiples of a fundamental conductance value. The fundamental conductance value is considered as the signature of single molecular conductance. This technique largely eliminates possible contamination by forming fresh electrode interfaces during junction breakage to which the local molecules can attach almost instantly. However, in the traditional SPMBJ technique,[11−14] the measured conductance complicates the interpretations due to the continuous modification of the contact configurations introduced by the continuous retraction of the SPM tip.[15,16] The conductance histograms constructed without the preselection process just show one or two broadened peaks, and the other detail characteristic features were smashed out by the introduced complexities of contact configuration changes.[11,17−19] Besides, with the traditional technique, only one kind molecule can be measured in a single experiment. The real experimental conditions can change from experiment to experiment, making it difficult to compare the results of different experiments.

Here we demonstrate a method to combine SPM nanolithography and the SPM break junction method to fabricate molecular junction devices and to characterize the electronic transport properties in greater detail (Figure 1). First, we

(1) Nitzan, A.; Ratner, M. A. *Science* **2003**, *300*, 1384–1389.
(2) Service, R. F. *Science* **2001**, *294*, 2442–2443.
(3) Chen, J.; Reed, M. A.; Rawlett, A. M.; Tour, J. M. *Science* **1999**, *286*, 1550–1552.
(4) Cui, X. D.; Primak, A.; Zarate, X.; Tomfohr, J.; Sankey, O. F.; Moore, A. L.; Moore, T. A.; Gust, D.; Harris, G.; Lindsay, S. M. *Science* **2001**, *294*, 571–574.
(5) Park, J.; Pasupathy, A. N.; Goldsmith, J. I.; Chang, C.; Yaish, Y.; Petta, J. R.; Rinkoski, M.; Sethna, J. P.; Abruna, H. D.; McEuen, P. L.; Ralph, D. C. *Nature* **2002**, *417*, 722–725.
(6) Reed, M. A.; Zhou, C.; Muller, C. J.; Burgin, T. P.; Tour, J. M. *Science* **1997**, *278*, 252–254.
(7) Slowinski, K.; Chamberlain, R. V.; Miller, C. J.; Majda, M. *J. Am. Chem. Soc.* **1997**, *119*, 11910–11919.
(8) Wold, D. J.; Frisbie, C. D. *J. Am. Chem. Soc.* **2001**, *123*, 5549–5556.
(9) Xu, B. Q.; Tao, N. J. *Science* **2003**, *301*, 1221–1223.
(10) Lindsay, S. M.; Ratner, M. A. *Adv. Mater.* **2007**, *19*, 23–31.
(11) Jang, S.-Y.; Reddy, P.; Majumdar, A.; Segalman, R. A. *Nano Lett.* **2006**, *6*, 2362–2367.
(12) Li, Z.; Kosov, D. S. *Phys. Rev. B* **2007**, *76*, 035415/1−035415/7.
(13) Tao, N. J. *Nat. Nanotechnol.* **2006**, *1*, 173–181.
(14) Venkataraman, L.; Klare, J. E.; Tam, I. W.; Nuckolls, C.; Hybertsen, M. S.; Steigerwald, M. L. *Nano Lett.* **2006**, *6*, 458–462.
(15) Lee, M. H.; Speyer, G.; Sankey, O. F. *Phys. Status Solidi B* **2006**, *243*, 2021–2029.
(16) Selzer, Y.; Allara, D. L. *Annu. Rev. Phys. Chem.* **2006**, *57*, 593–623.
(17) Chen, F.; Hihath, J.; Huang, Z.; Li, X.; Tao, N. J. *Annu. Rev. Phys. Chem.* **2007**, *58*, 535–564.
(18) González, M. T.; Wu, S.; Huber, R.; van der Molen, S. J.; Schönenberger, C.; Calame, M. *Nano Lett.* **2006**, *6*, 2238–2242.
(19) Chen, F.; Li, X.; Hihath, J.; Huang, Z.; Tao, N. *J. Am. Chem. Soc.* **2006**, *128*, 15874–15881.

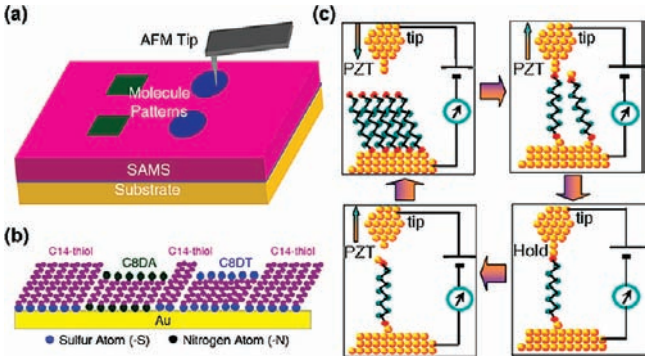

Figure 1. Schematics of AFM nanografting (a and b) and conductance measurements using modified SPMBJ techniques (c).

patterned thiol- and amine-terminated *N*-alkane ($N = 6, 8, 10$) molecules in the tetradecanethiol ($CH_3(CH_2)_{13}SH$) (C14-thiol) monolayer matrix using the AFM nanografting technique which is widely used to manipulate the molecule and modulate the function of the molecule on bare or molecule coated substrates. And then we used a modified SPMBJ technique to characterize the electronic transport properties in situ. The modification on the traditional SPMBJ technique would minimize the influence of continuous STM tip retraction on the electron transport through the molecular junction in the monitoring process. This method allows us to investigate the details of the electron transport properties of multiple molecules under the same experiment with exactly the same experimental conditions.

N-Alkanes (*N* is the number of methylene groups) we chose in this work have a rather large HOMO−LUMO gap which does not vary significantly with molecular length by changing *N*. Therefore, it is easier to isolate the molecule−electrode contact effects from other factors from the molecules themselves. Besides, several helpful discussions have been introduced to illustrate the contact effects on the electron transport through the molecules based on *N*-alkane molecules.[19−23] In those previous works, multiple single molecular conductance groups have been reported due to the different contact conformations. Here, by systematically measuring and comparing the conductance of the *N*-alkanes with different terminated anchoring groups, thiol (−SH) and amine ($-NH_2$), on the same substrate, one can gain further insights into the conduction mechanisms of the molecular junctions involving the consideration of contact effects.

Experimental Details

Chemicals. The 1-tetradecanethiol (C14-thiol), α,ω-alkanedithiols, and α,ω-alkanediamines: 1,6- hexanedithiol (C6DT), 1,8-octanedithiol (C8DT), 1,10-decanedithiol (C10DT), 1,6-hexanediamine (C6DA), 1,8-octanediamine (C8DA), and 1,10-decanediamine (C10DA) were purchased from Aldrich(reagent grade) and used without further purification.

For gold substrate coating, the gold beads used are from the Kurt J. Lesker company (99.999%), and the mica sheet (Grade V1) was from Ted Pella Inc. The gold wires for the STM tip (diameter: 0.25 mm, 99.999%) are from Alfa Aesca.

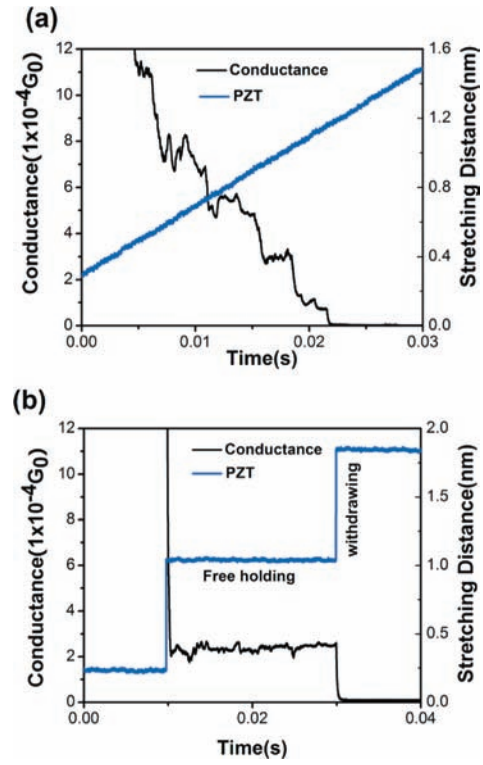

Figure 2. Representative conductance traces obtained with the traditional STMBJ technique (a) and modified STMBJ with abrupt stretching (withdrawing) and free holding processes (b).

All the other chemicals used in this study were purchased from commercially available sources (VWR, Sigma-Aldrich and Alfa Aesar) and used directly as received.

AFM Nanografting Technique. The SPM setup used in the experiments is the PicoPlus SPM system (Molecular Imaging) using the Pico Scan 3000 Controller (Molecular Imaging).

To fabricate the molecular junction devices, we used an AFM nanografting technique[24,25] (Figure 1a). The Au substrate was prepared by thermally evaporating a 120 nm thick gold layer on each freshly cleaved mica surface and then kept in a vacuum chamber to protect it from contamination. The substrate was kept at 420 °C, and the gold evaporation rate was kept at 0.6 Å/s during the evaporations. Before each experiment, it was annealed in a hydrogen flame to form Au(111) and immediately immersed in the solution with 1 mM (C14-thiol) in toluene to form a C14-thiol self-assembled monolayer (SAM).

AFM nanoshaving was used to make four markers on the C14-thiol SAM to facilitate the following nanolithography of alkanediamine and alkanedithiol molecules. In this process, the AFM tip with a spring constant of 40 N/m was used to apply a large force (~6 μN) on the substrate, which is able to make those markers deep enough to be identified with an integrated optical microscope. Once the markers were made, the sample was completely rinsed with ethanol and DI water and then dried with nitrogen gas. Immediately, 1 mM C8DA dissolved in 18 MΩ water was put on the sample inside a Teflon sample cell cleaned with boiling Piranha solution prior to the experiments. Then the sample was scanned to find an area within the markers for nanografting (Supporting Information, Figure S1). Figure 1a and b schematically show C8DA and C8DT molecule patterns fabricated using the AFM nanografting method subsequently in the C14-thiol SAM. The two square areas

(20) Müller, K. H. *Phys. Rev. B* **2006**, *73*, 045403/1−045403/6.
(21) Li, X. L.; He, J.; Hihath, J.; Xu, B. Q.; Lindsay, S. M.; Tao, N. J. *J. Am. Chem. Soc.* **2006**, *128*, 2135–2141.
(22) Li, C.; Pobelov, I.; Wandlowski, T.; Bagrets, A.; Arnold, A.; Evers, F. *J. Am. Chem. Soc.* **2008**, *130*, 318–326.
(23) Fujihira, M.; Suzuki, M.; Fujii, S.; Nishikawa, A. *Phys. Chem. Chem. Phys.* **2006**, *8*, 3876–3884.
(24) Kraemer, S.; Fuierer, R. R.; Gorman, C. B. *Chem. Rev.* **2003**, *103*, 4367–4418.
(25) Xu, S.; Miller, S.; Laibinis, P. E.; Liu, G.-y. *Langmuir* **1999**, *15*, 7244–7251.

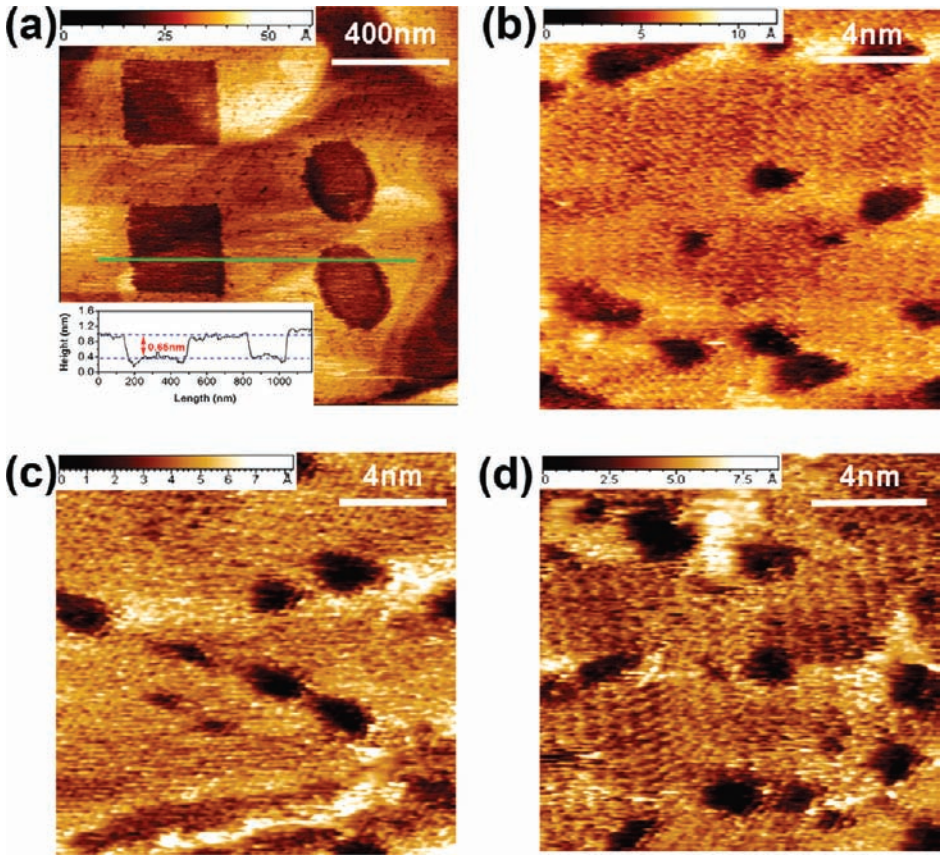

Figure 3. High resolution images of molecular SAMs. (a) AFM nanografted patterns of C8DA (two squares of 250 nm × 250 nm) and C8DT (two circles with diameter of 200 nm). The insert is cross section image labeled by the green line. The height difference between C14 and C8 SAMs is 0.65 nm. (b−d) Molecular resolution image of C14-thiol SAM (b), C8DA SAM (c), and C8DT SAM (d), with an ∼5 Å lattice constant.

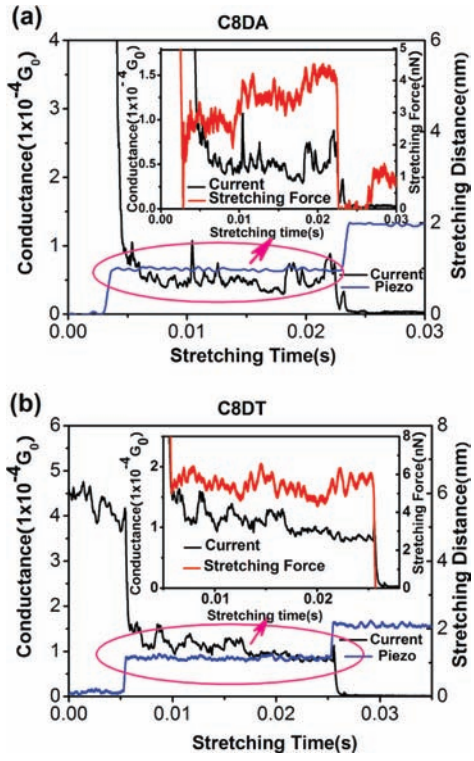

Figure 4. Typical conductance and force traces of molecular junctions. A conductance trace showing a plateau (a) for C8DA and (b) for C8DT single molecule junction, corresponding with the "holding" stage of the stretching process. Inserts show the conductance and stretching force curves.

of C14-thiol SAMs were removed and replaced first by C8DA molecules by mechanical displacement with an AFM tip with a spring constant of 0.27 N/m under water solution containing C8DA. For nanografting, the typical force used in our experiments ranges from 10 to 20 nN depending on the sharpness of the tip, and we found this range of force is sufficient to remove the C14-thiol molecules for replacement by the C8DA molecules without damaging the underneath Au(111) surface. After nanografting for ∼30 min and subsequent 3 h self-assembly and *in situ* scanning, the sample was rinsed with DI water and dried again for C8DT nanografting. C8DT molecules were patterned following the similar steps under toluene containing 1 mM C8DT in the two circular areas. The accomplished sample chip is rinsed with ethanol and DI water after another 3 h of self-assembly. Then the sample was put into pure toluene after being dried with nitrogen and was then ready for the electronic transport properties study with modified SPMBJ techniques.

Modified SPMBJ Technique. For the traditional SPM break junction technique, the Au-coated SPM tip was first driven toward an Au substrate covered with sample molecules by the software-controlled piezoelectric transducer (PZT) until the current reaches a preset value, indicating the formation of the Au−molecule−Au junctions. Then the SPM tip retracted continuously, and the electron transport properties of molecular junctions were monitored simultaneously (Figure 2a). To minimize the contact conformation complexities arisen from the bare SPM tip retraction, here we divided this continuous retraction process into two processes (Figure 1c): *abrupt stretching and free holding of the molecular junctions*. In the abrupt stretching process, the tip is withdrawn abruptly for ∼8 Å. Then, the tip is held stable at that position for 20 ms, and so the conductance of molecules can be measured without the retracting movements of the tip until the next abrupt withdrawal (Figure 2b). The abrupt stretching and free holding processes are

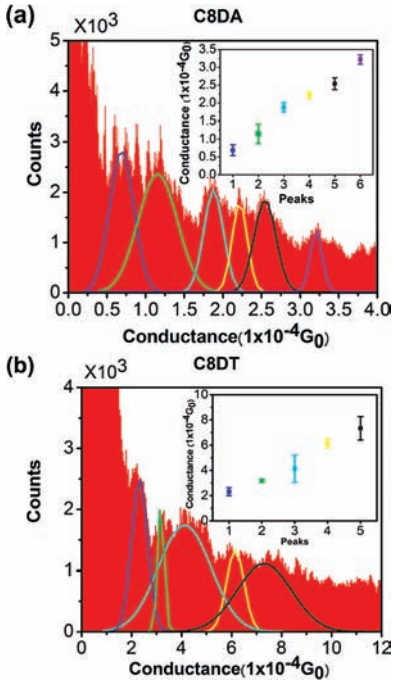

Figure 5. Integrated conductance histogram constructed without any selections for C8DA (a) and for C8DT (b) molecular junctions; the color curves are the Gaussian fitting for each enhanced peak. The inserts show the center conductance value enhanced peaks obtained by the Gaussian fitting. The standard deviations, the full widths at half-maximum height (fwhm) of the peaks, estimated for each peak from the Gaussian fitting are marked as error bars. Noticeably, the first peaks of the Gaussian fitting in (a) and (b) agree with the results obtained from traditional STMBJ.

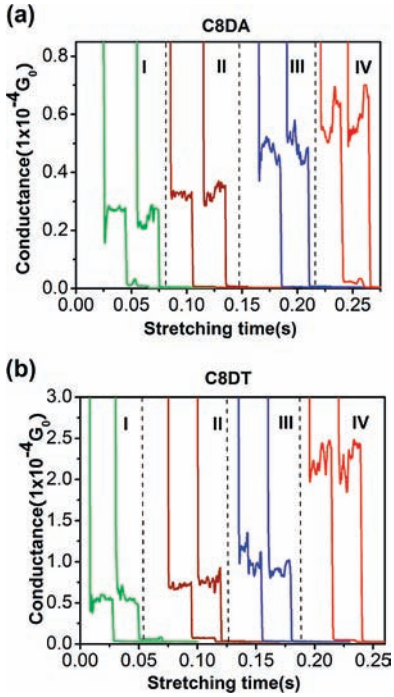

Figure 6. Representative conductance trances for the four groups of C8DA (a) and C8DT (b) molecular junctions.

utilized alternatively until the molecular junctions are completely broken. The processes were controlled by a homemade LabView computer program.

The conducting SPM tip was made of Si (Nanoscience Instruments) coated with a 15 nm layer of chromium and then a 35 nm

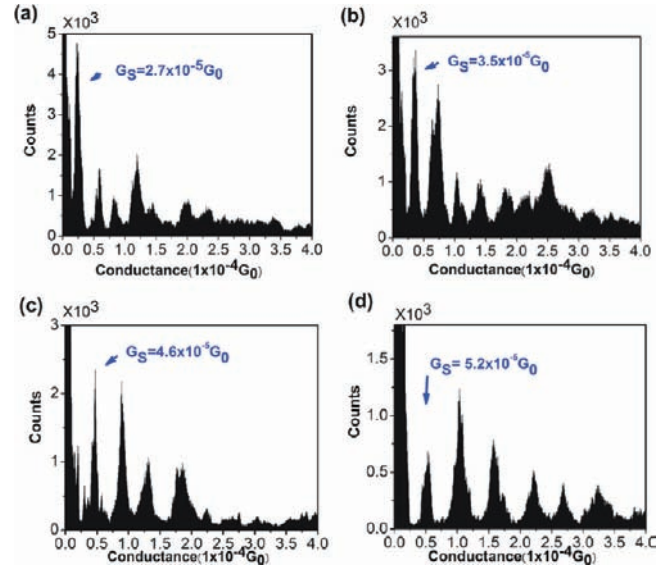

Figure 7. Histogram constructed separately with each single molecular conductance set of C8DA $G_{S1} = 2.7 \times 10^{-5}G_0$ (a), $G_{S2} = 3.5 \times 10^{-5}G_0$ (b), $G_{S3} = 4.6 \times 10^{-5}G_0$ (c), and $G_{S4} = 5.2 \times 10^{-5}G_0$ (d).

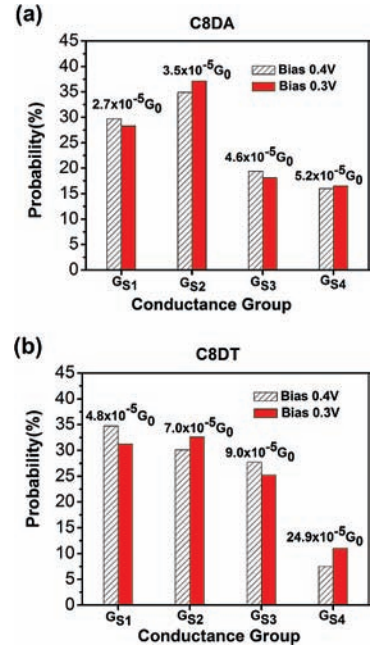

Figure 8. Corresponding probabilities of the four different conductance groups for C8DA (a) and C8DT (b) molecular junctions.

layer of gold (99.999%) using an ion beam coater (Gatan model 681) before each measurement. The spring constant of the AFM cantilever was calibrated to be ~40 N/m.

Results and Discussions

Molecular Patterns with Nanografting. After nanografting, the high resolution AFM images were obtained without damaging the SAM patterns under the low force (typical 0.2−0.5 nN) applied. Figure 3a (1300 nm ×1300 nm) shows two square (250 nm × 250 nm) C8DA and two circular (diameter of ~200 nm) C8DT molecular patterns nanografted in the C14-thiol SAM. Au(111) terraces were clearly seen, indicating that only the C14-thiol molecular layer is removed and replaced while the substrate was kept intact in the nanografting process. Molecular resolution

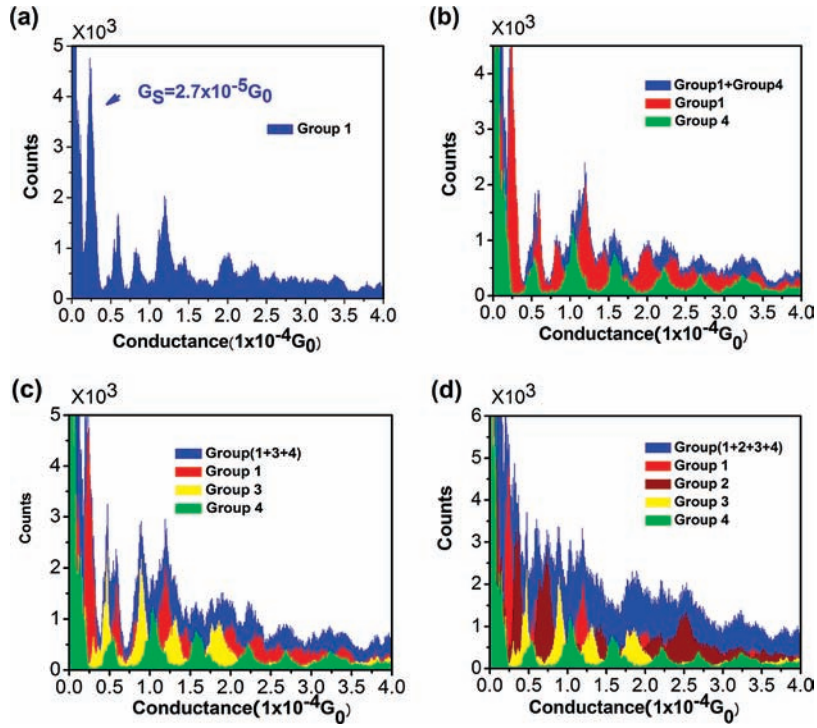

Figure 9. Mechanisms of C8DA integrated histogram formed from different conductance groups. Histogram of Group 1, $G_S = 2.7 \times 10^{-5}G_0$ (a); histogram constructed with combination (blue) of Group 1 (red) and Group 4 (green) (b); histogram constructed with combination (blue) of Group 1 (red), Group 4 (green), and Group 3 (yellow) (c). Integrated histogram constructed with all curves with conductance plateaus involve Group 1 (red), Group 4 (green), Group3 (yellow), and Group2 (wine) (d).

AFM images (15 nm × 15 nm) of C14-thiol (Figure 3b) and C8DA (Figure 3c) reveal a two-dimensional close-packed structure with a lattice constant of ~5.0 Å, consistent with the well-known (3 × 3)R30° based structure.[26,27] Figure 3d, the molecular resolution AFM image (15 nm × 18 nm) of C8DT, however, shows an additional domain of the head-to-head packing arrangement.[28] The mostly close-packed "stand-up" SAM domain suggests that replacement of molecules was spatially confined, having a limited area to insert them into the exposed gold surface areas.[29] Therefore, as is shown in Figure 3a, the average height difference measured between C14-thiol and C8DT or C8DA area is ~0.65 nm, which is almost the length difference between C14 and C8 molecules. Therefore, by using the AFM nanolithography technique, we fabricated the single molecule junction devices of both C8DA and C8DT molecules on the same substrate for the study of their electronic transport properties under exactly the same experimental conditions.

Conductance Measurements. To measure the conductance of molecules with the modified SPMBJ technique, first we scan to locate the molecule patterns (alkanedithiol or alkanediamine).

Figure 4a and b show the conductive-AFM stretching (piezo) distance and the typical conductance traces corresponding to the stretching, with a plateau lifetime up to ~20 ms, agreeing with the lasting time of the holding process and is much longer than those obtained with traditional SPMBJ. With the longer lifetime, the plateaus become much more distinct and well-defined, indicating the formation and maintenance of stable molecular junctions without continuous mechanically induced contact changes introduced by the retracting movement of the tip. The conductance and force traces in the inserts show synchronized fluctuations of both conductance and force during the free hold process, indicating that the contact conformation changes in the contacts lead to the fluctuation of conductance.[20,30−33] Among ~1200 C8DA conductance traces obtained with modified SPMBJ under a bias voltage of 0.4 V, 1050 traces show well-defined plateaus (Figure 4a), while 904 out of 1200 traces show well-defined plateaus for C8DT (Figure 4b). We constructed the conductance histograms of C8DA and C8DT based on the traces with well-defined plateaus without any selection (Figure 5a and b). The histogram of C8DA and C8DT both show several enhanced peaks. By Gaussian fitting (the color curves in Figure 5) those enhanced peaks shown in the histograms of C8DA and C8DT, the centered conductance values represented by those peaks are shown in the inserts of Figure 5 with error bars representing the distributions of each peak. For C8DA and C8DT, the first enhanced peaks are shown at $5.2 \times 10^{-5}G_0$ (C8DA) and $24.9 \times 10^{-5}G_0$ (C8DT), which are close to the single molecular conductance values reported in previous work with the traditional STMBJ technique.[9,14] However, the following new specific phenomena are observed with the modified technique: (1) Without any preselections, the histograms of C8DA and C8DT both show several *enhanced peaks* compared to only one or two broadened peaks in the

(26) Dubois, L. H.; Nuzzo, R. G. *Annu. Rev. Phys. Chem.* **1992**, *43*, 437–463.
(27) Fenter, P.; Eberhardt, A.; Eisenberger, P. *Science* **1994**, *266*, 1216–1218.
(28) Cavallini, M.; Bracali, M.; Aloisi, G.; Guidelli, R. *Langmuir* **1999**, *15*, 3003–3006.
(29) Xu, S.; Laibinis, P. E.; Liu, G.-y. *J. Am. Chem. Soc.* **1998**, *120*, 9356–9361.
(30) Basch, H.; Cohen, R.; Ratner, M. A. *Nano. Lett.* **2005**, *5*, 1668–1675.
(31) Xu, B. Q. *Small* **2007**, *3*, 2061–2065.
(32) Xu, B. Q.; Xiao, X. Y.; Tao, N. J. *J. Am. Chem. Soc.* **2003**, *125*, 16164–16165.
(33) Andrews, D. Q.; Duyne, R. P. V.; Ratner, M. A. *Nano Lett.* **2008**, *8*, 1120–1126.

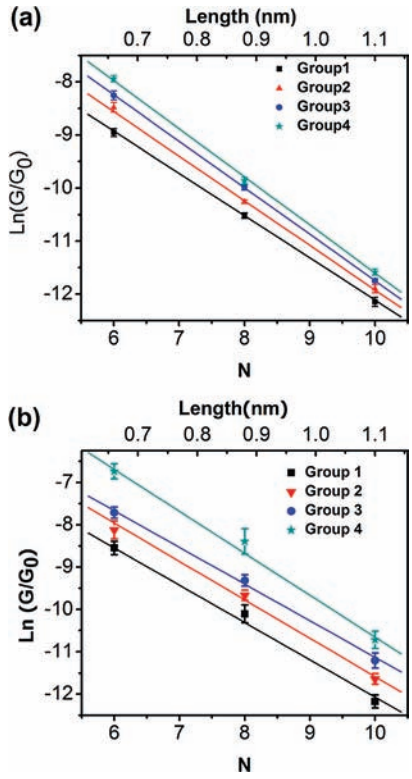

Figure 10. Natural logarithm of conductance vs molecule length for the four conductance groups of C8DA (a) and C8DT (b) single molecule junction.

integrated histograms obtained with the traditional SPM break junction technique.[11,19] (2) For C8DT, the histogram shows the additional peaks that do not locate at the integer multiple positions of any of the other peaks. (3) Although several enhanced peaks in the C8DA histograms do locate at or close to the integer multiple positions of the first peaks, some of them show an identifiable shift. Noticeably, besides the enhanced peaks in the C8DA histograms, there are some thin peaks, which are located away from the integer multiple positions of the first peak. Some of them are even smaller than the previously reported single molecular conductance ($5.4 \times 10^{-5}G_0$) of C8DA.

Grouping Method. To explain those new phenomena above, we went through all the traces carefully and identified four different fundamental plateaus for both C8DA and C8DT (Figure 6a and b). The conductance values corresponding to these fundamental plateaus are not integer multiples of each other. Meanwhile, for all conductance traces with plateaus, the conductance values are found to be an integer multiple of one of these four fundamental ones. As a result, all conductance traces with plateaus can be divided into four groups, 1 to 4. The histograms constructed using the conductance traces of each group for C8DA are shown in Figure 7, and similar results were found for C8DT (Figure S2 in the Supporting Information). In each of the histograms in Figure 7, 6−9 pronounced peaks can be identified.

The first peak in each of the histograms represents the fundamental conductance value belonging to the group, and the other peaks locate at the integer multiple position of this fundamental one. Those fundamental values are used as the signature of single molecular conductance. Considering the simple and stable structure and conformation of an alkane molecule, the variations of a single molecular conductance value should be attributed to the different contact configurations during the formation of the molecular junctions as both theoretical and experimental results suggested.[32,34−36]

Recent experimental studies resolved two and three different sets of conductance values for a single molecule, and they were believed to be responsible for different contact configurations of the molecular junctions.[17,21,22,37] In this study, we observed extra single molecular conductance groups for both C8DA and C8DT with the modified technique. By minimizing the contact conformation changes introduced by continuous SPM tip retraction in the traditional technique, the small differences between conductance groups can be identified. Although, in some theoretical discussions, even more sets of conductance for the single molecule should coexist due to different gold atomic configurations of the electrodes,[20,38] fewer discussions consider the stabilities of different atomic configurations in real systems. Our results suggest that only some specific conformations are in optimal states and stable enough to be realized repeatedly during the formation of molecular junctions. As is discussed above, the four different conductance groups are related to the four preferential stable contact conformations. There may be some other preferential contact conformation groups, but their conductance values are so close to those four groups that they cannot be identified experimentally.

Moreover, because of the similar structure of C8DA and C8DT, each preferential contact conformation should also have a similar gold atom arrangement.[39] It was also reported that, in contrast to the thiol−Au bond, the amine−Au bond is weaker but more rigid[40] which would lower the conductance value and narrow the distributions of conductance variations.[14,33] The four sets of single molecular conductance for both C8DA and C8DT reflect the similar gold atom arrangement of the electrodes of the contacts, while different values of their corresponding conductance can be attributed to the strength of the thiol−Au and amine−Au bonds. Although more theoretical and experimental studies are needed to discuss the detailed mechanisms of formation of stable contact conformations, the current results provide significant new insights into the effect of contact conformation on the electrical transport through molecular junctions.

For the first two or three conductance peaks shown in histograms, the peak can be identified as two or three molecules parallel to each other with identical contact configurations. However, to consider the peaks located at the higher integer multiple of the fundamental conductance values, such as $5G_{S1}$, the reason for forming identical contact configurations for so many parallel molecules is not easily understood so far. Another possibility is that the higher multiple peaks located in the histograms come from the parallel molecules with different contact configurations. For example, the $6G_{S2}$ of C8DA, $21 \times 10^{-5}G_0$, can also be considered to be formed by four molecules from group1 and two molecules from group 4, $4G_{S1} + 2G_{S4} = 21.2 \times 10^{-5}G_0$. Further studies are still needed for a complete understanding of electron transport mechanisms when many molecules are parallel between electrodes in the molecular junctions.

(34) Grigoriev, A.; Sköldberg, J.; Wendin, G.; Crljen, Ž. *Phys. Rev. B* **2006**, *74*, 045401/01−045401/16.
(35) Ke, S. H.; Baranger, H. U.; Yang, W. *J. Chem. Phys.* **2005**, *123*, 114701/01–114701/08.
(36) Kondo, H.; Kino, H.; Nara, J.; Ozaki, T.; Ohno, T. *Phys. Rev. B* **2006**, *73*, 235323/01–235323/10.
(37) Morita, T.; Lindsay, S. *J. Am. Chem. Soc.* **2007**, *129*, 7262–7263.
(38) Grönbeck, H.; Häkkinen, H. *J. Phys. Chem. B* **2007**, *111*, 3325–3327.
(39) Quek, S. Y.; Venkataraman, L.; Choi, H. J.; Louie, S. G.; Hybertsen, M. S.; Neaton, J. B. *Nano Lett.* **2007**, *7*, 3477–3482.
(40) Fagas, G.; Greer, J. C. *Nanotechnology* **2007**, *18*, 424010/1–424010/4.

Table 1. Decay Constant β_N (β_L) and Contact Resistance R_c of the Four Conductance Groups for Both C8DA and C8DT

	C8DA				C8DT			
group	β_N	β_L (Å^{-1})	ln A_G	R_c (kΩ)	β_N	β_L (Å^{-1})	ln A_G	R_c (kΩ)
1	0.82 ± 0.02	0.68 ± 0.02	−4.11	787.4	0.90 ± 0.05	0.75 ± 0.05	−3.28	345.9
2	0.85 ± 0.03	0.71 ± 0.02	−3.36	372.0	0.87 ± 0.03	0.73 ± 0.02	−2.77	206.5
3	0.86 ± 0.02	0.72 ± 0.02	−3.02	264.7	0.87 ± 0.02	0.73 ± 0.02	−2.34	134.3
4	0.89 ± 0.05	0.74 ± 0.02	−2.42	145.2	1.01 ± 0.04	0.84 ± 0.04	−0.43	19.8

Probabilities of Each Conductance Set. To further understand the influence of anchoring terminated groups on electron transport through the molecular junctions and to relate the specific features in the integrated histogram (using all the conductance traces with plateaus) to each single molecular conductance set, the probabilities (ratio of the number of conductance traces in each conductance group to that of all selected traces) for the preferential contact configurations are also counted (Figure 8a and 8b). Under bias 0.3 and 0.4 V, the corresponding probability diagrams of the molecule with the same anchoring linkers show similar distributions but show a discrepancy for the different anchoring linkers. These results imply that variations of conductance of molecular junctions root from the molecule electrode contact configuration variations of the molecules while the alkane parts of the molecules do not alter the conductance significantly. Figure 9 demonstrates how the integrated histogram was constructed by involving each conductance group one by one. For C8DA (Figure 9), only group 1 ($2G_{S1}$ is close to the G_{S4}) can enhance the peak of group G_{S4} (totaled probability ∼45%) and the integrated histogram only shows enhanced peaks located at integer multiples of $\sim 5.4 \times 10^{-5} G_0$ (Figure 9 a), agreeing with the previous experiment results of single molecule conductance of C8DA.[14] However, as the probability of other peaks are close (e.g., group 2 has a probability of 34%) to the integrated probabilities (Figure 9c and d), the other peaks are also clearly shown in the Figure 5a. In contrast, for C8DT (Figure S3 in the Supporting Information), G_{S4} ($24.9 \times 10^{-5} G_0$) is close to $5G_{S1}$ and group $3G_{S2}$. Therefore, in the histogram, the 24.9×10^{-5} G_0 peak was greatly enhanced (totaled probability over 70%) and the other peaks were almost dimished. These results directly show why only one or two broadened peaks were observed in the histogram when all conductance traces were selected in previous work[11,17,18] and imply that the preselection processes may lose some important information in the formation of the molecular junctions (Figure 9).

Contact Resistance. With large HOMO−LUMO gaps, the electronic transport mechanism through saturated molecules of alkanes is electron tunneling[8,20,41] and obeys the following equations:

$$G/G_0 = A_G \exp(-\beta_L L) = A_G \exp(-\beta_N N) \quad (1)$$

and

$$\ln(G/G_0) = -\beta_L L + \ln A_G = -\beta_N N + \ln A_G \quad (2)$$

where $G_0 = 2e^2/h$ is the conductance quantum and the decay constants β_N (β_L) are mainly determined by the molecule itself and keep constant with the number of methylene groups (length of molecule) under a certain contact conformation. As is reported in previous works,[19,21] for *N*-alkane molecules, the β determined with different conductance sets, indicating the different contact configurations, show almost the same results (0.8−1.0). The intercept ln A_G, on the other hand, should be mostly related to the contact potential that corresponds to the different contact conformations.[40] Therefore, the expression of the contact resistance can be written as

$$R_c = 1/(A_G G_0) \quad (3)$$

We measured the conductance of alkanedithiol and alkanediamine molecules with 6, 8, and 10 carbon atoms to determine the decay constants β of different single molecular conductance sets with different contact configurations. Figure 10 shows ln(G/G_0) vs the molecule length for each conductance group (Figure 10a for alkanediamines and Figure 10b for alkanedithiols).

The intercept ln A_G of each conductance set can be obtained by extrapolating the fitting line to $N = 0$ (length = 0). Contact resistances are calculated with eq 3. It is interesting to note that the contact resistance values of alkanedithiol molecular junctions are smaller than the contact resistance values of their counterpart alkanediamine molecular junction, suggesting that a stronger bond of the molecule−electrode contact reduces the contact resistance (see Supporting Information for details).

However, the tunneling decay constants (β_N (β_L)) are found to be approximately the same (∼0.8 to 0.9 per carbon atom) not only for different conductance groups within the same termini groups (-thiol or -amine) but also for different termini groups (-thiol and -amine). This result, in agreement with the previous work,[14,19,21] clearly indicates that the decay constant (β_N (β_L)) is mostly determined by the molecules bridged between the electrodes themselves and is only slightly influenced by the contact configuration (Table 1).

Summary and Conclusions

We have demonstrated a new method to combine SPM nanolithography and modified SPM break junction techniques to fabricate and characterize single molecular break junction devices. It allows one to eliminate, or at least minimize, the variations of experimental conditions and enables the measurement of multiple molecules with exactly the same experimental conditions.

By patterning alkanedithiol and alkanediamine molecules in the alkanethiol template, the conductance mechanisms of the two kinds of molecular junctions are studied with modified SPMBJ techniques. To minimize the contact conformation changes introduced with continuous SPM tip retraction in the traditional SPMBJ methods, we introduced the new "stretching-holding" approaches. With the modified technique, the small difference between different conductance sets can be identified with more stable molecular junctions formed. Multiple groups of conductance values are found indicating the coexistence of several preferential and related stable contact conformations during the formation of molecular junctions.

(41) Holmlin, R. E.; Haag, R.; Chabinyc, M. L.; Ismagilov, R. F.; Cohen, A. E.; Terfort, A.; Rampi, M. A.; Whitesides, G. M. *Annu. Rev. Phys. Chem.* **2001**, *123*, 5075–5085.

By analyzing the probabilities of different conductance sets, we discussed the specific new features in the integrated histograms. The results imply the preselection process in some previous work may lose some important contact configuration information. We also investigated electronic transport property changes with the molecular length. For different conductance sets of the same kind of molecules, the similar decay constants and different contact resistances provide more evidence to support that the conductance differences among each set are due to the molecule−electrode contact configuration differences.

Acknowledgment. We thank Anna Jagielska for useful discussions and gratefully acknowledge the National Science Foundation (ECCS 0823849) for financial support.

Supporting Information Available: Experimental details, AFM nanolithography, conductance grouping methods, and data analysis results. This material is available free of charge via the Internet at http://pubs.acs.org.

JA900989A